Civil Engineering Dimension, Vol. 25, No. 1, March 2023, 10-19
ISSN 1410-9530 print / ISSN 1979-570X online
DOI: https://doi.org/10.9744/CED.25.1.10-19

Seismic Performance Comparison of Simply Supported Hollow Slab on Pile Group Structure with Different Operational Category and Shear Panel Damper Application

Haroki, Y.[1], Awaludin, A.[1]*, Priyosulistyo, H.[1], Setiawan, A.F.[1], and Satyarno, I.[1]

Abstract: This study is aimed to compare the seismic performance of simply supported hollow slab on pile group (SHSPG) structures designed as "critical" and "essential" viaducts with shear panel damper (SPD) devices. There were three numerical models to be compared, namely SHSPG-A, SHSPG-B, and SHSPG-C. SHSPG-A is a "critical" viaduct with 35 piles per one pile head. SHSPG-B is an "essential" viaduct with 18 piles per one pile head. SHSPG-C is an "essential" viaduct with 18 piles per one pile head plus sixteen SPDs. Numerical models considered the prestressing effect of the spun pile. Nonlinear time history analyses were executed using seven pairs of recorded ground motions that had been scaled and adjusted to the seismic characteristics of Yogyakarta, Indonesia. As the result, the performance level of SHSPG-A was much better than SHSPG-B. The SPDs application could maintain SHSPG-C's performance at the same level as SHSPG-A and dissipate 34.28%-53.03% of the seismic energy.

Keywords: Numerical model, prestress effect, nonlinear time history analysis, energy dissipation.

Introduction

Pile-supported slab viaduct is commonly used in soft soil sites. The structure consists of spun pile group, pile head, and slab. The use of fabricated spun piles can achieve high consistency of the structure and reduce material, labor costs, and construction time [1]. However, it has the disadvantages of low energy dissipation, sudden collapse, and brittle failure [2,3].

Most of the Indonesia region has a high potential for shallow earthquakes with a hypocenter depth of less than 60 km [4]. To accommodate large earthquakes, the pile-supported slab viaduct structure is designed as a "critical" viaduct with a response modification factor (R) value of 1.5. As the result, the structure has to withstand a large seismic load and has a high level of seismic performance. The consequence is that the structure requires many piles. The number of piles can be reduced by downgrading the operational category to an "essential" viaduct with an R-value of 3.5. However, its performance level will be lower than the structure designed under the "critical" viaduct category.

The seismic performance of the pile-supported slab viaduct structure can be upgraded by adding shear panel damper (SPD) devices [5]. The SPD device is made of low-yield point steel with low-yield strength and high elongation that can dissipate seismic energy [6,7]. Its use as a hysteretic damping device has several advantages, such as easy installation, easy maintenance, and affordable prices [8]. Unfortunately, SPD cannot withstand gravity loads, so SPD needs to be used in parallel with an elastomeric rubber bearing (ERB) device that can accommodate gravity loads.

This study proposed a simply supported hollow slab on a pile group structure, namely SHSPG, designed as an "essential" viaduct and equipped with SPD devices. The "critical and "essential" SHSPG structures were simulated numerically using the nonlinear time history (NLTH) analysis method. The NLTH analyses were executed based on recorded ground motion from other locations which were scaled and adjusted to the seismic characteristics of Yogyakarta. The studied parameters were the displacement response of the piles, moment-curvature of the plastic hinges, seismic performance of the structures, and energy distribution of the structures.

Method

Properties of the Structures

The spun pile is concrete with prestressed steel bars, generally known as PC bars. The compressive strength of the concrete is 52 MPa, while the yield and ultimate strength of the PC bar are 1387 MPa and 1455 MPa, respectively. The outer diameter of the spun pile is 600 mm and the inner diameter is 400 mm. The diameter of the PC bar is 9.2 mm. The compressive strength of the hollow slab concrete is 52 MPa, while the compressive strength of the pile head concrete is 33 MPa. The cross-section of the spun pile, hollow slab, and pile head were shown in Figure 1.

[1] Department of Civil and Environmental Engineering, Universitas Gadjah Mada, Yogyakarta, INDONESIA
*Corresponding author; Email: ali.awaludin@ugm.ac.id

Note: Discussion is expected before July, 1st 2023, and will be published in the "Civil Engineering Dimension", volume 25, number 2, September 2023.

Received 20 December 2022; revised 23 February 2023; accepted 15 March 2023.

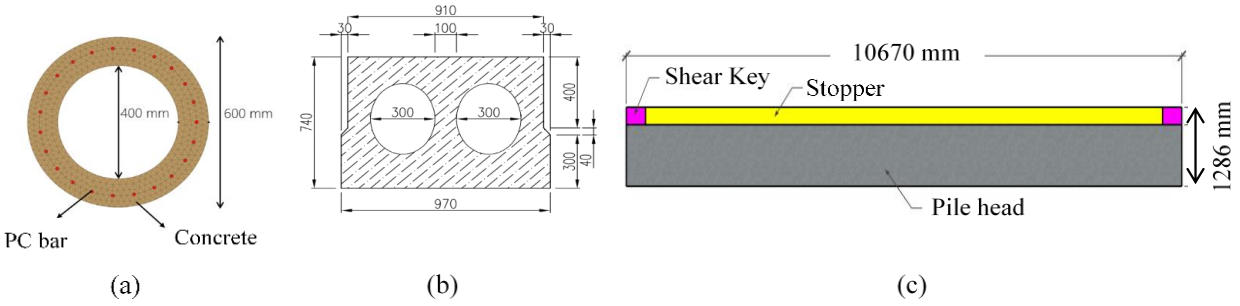

Figure 1. Cross-Section: (a) Spun Pile; (b) Hollow Slab; (c) Pile Head

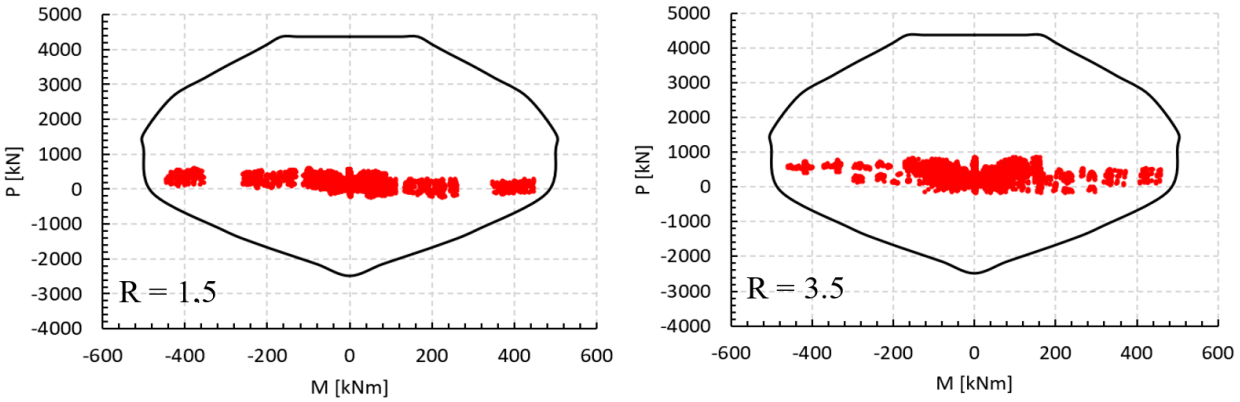

Figure 2. P-M Interaction Diagrams of Spun Pile

Table 1. Concrete Material Properties

f_{pc} (MPa)	e_{psc0}	f_{pcu} (MPa)	e_{psu}	λ	f_t (MPa)	E_{ts} (MPa)
-52	-0.002	10.40	0.00322	0.071	4.33	2737

Table 2. PC Bar Material Properties

f_y (MPa)	b	E (MPa)	ε_{max}	ε_{min}
1387	0.01988	220267	0.017	-0.017

Design of The Structures

The SHSPG structures were designed following PM 60-2012 entitled *Persyaratan Teknis Jalur Kereta Api* (Railway Technical Requirement) [9]. The seismic design of the viaduct structure was arranged in SNI 2833-2016 [10]. The values of response modification factors are 1.5 for the "critical" viaduct and 3.5 for the "essential" viaduct [11]. The span and dimensions of the slab structure are referred to *detailed engineering design* (DED) of the Yogyakarta International Airport Railway project. Based on the elastic design, the "critical" SHSPG requires 35 piles per one pile head, while the "essential" SHSPG requires 18 piles per one pile head. The P-M interaction diagrams of the spun piles are shown in Figure 2.

Material Model

Concrete and PC bar materials of the spun pile were modeled by considering their linear and nonlinear parameters. Concrete material followed Kent & Park model for unconfined concrete [12]. The input parameters of the concrete model were compressive strength (f_{pc}), strain at maximum strength (e_{psc0}), crushing strength (f_{pcu}), strain at crushing strength (e_{psu}), the ratio between unloading slope and initial slope (λ), tensile strength (f_t), tension softening stiffness (E_{ts}), and initial stress (σ_0) as summarized in Table 1. PC bar material was modeled as bilinear material with a certain strain limit. Its parameters were yield strength (f_y), strain hardening ratio (b), initial elastic tangent (E), strain at maximum tensile strength (ε_{max}), and strain at maximum compressive strength (ε_{min}) as shown in Table 2. Prestress effects on both concrete and PC bar were considered and assigned as initial stress of material with the values of -10.57 MPa for the concrete material and 1040 MPa for the PC bar material. Pile head and hollow slab concrete materials were modeled elastically with elastic tangent values of 27081 MPa and 33234 MPa because this study was focused to evaluate the nonlinear behavior of spun pile elements. This assumption was validated by checking the concrete strain after the analyses were done.

Fixity Depth of Spun Pile

In order to simplify the structure models, a preliminary analysis should be executed using Scientific ToolKit for OpenSees (STKO) software. In this preliminary analysis, a whole pile supported by nonlinear soil springs along the embedded part was modeled. The pile was modeled with 4000 mm length of the free head part and 30000 mm length of the embedded part. Soil data were obtained from the borlog test at the project location. The nonlinear soil spring included the tip resistance, the axial resistance, and the horizontal resistance. Based on the numerical analysis result in Figure 4, the fixity point was the point that experiences the maximum bending moment which was located at 5000 mm under the ground surface. This was reasonable because the analytical result showed a range value of 4933-5187 mm. In structure models, the spun pile was only modeled from the top to the fixity point without nonlinear soil spring. This simplification could save more time and memory file during NLTH analysis.

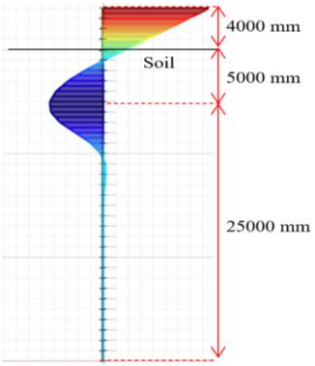

Figure 4. Fixity Depth of Spun Pile

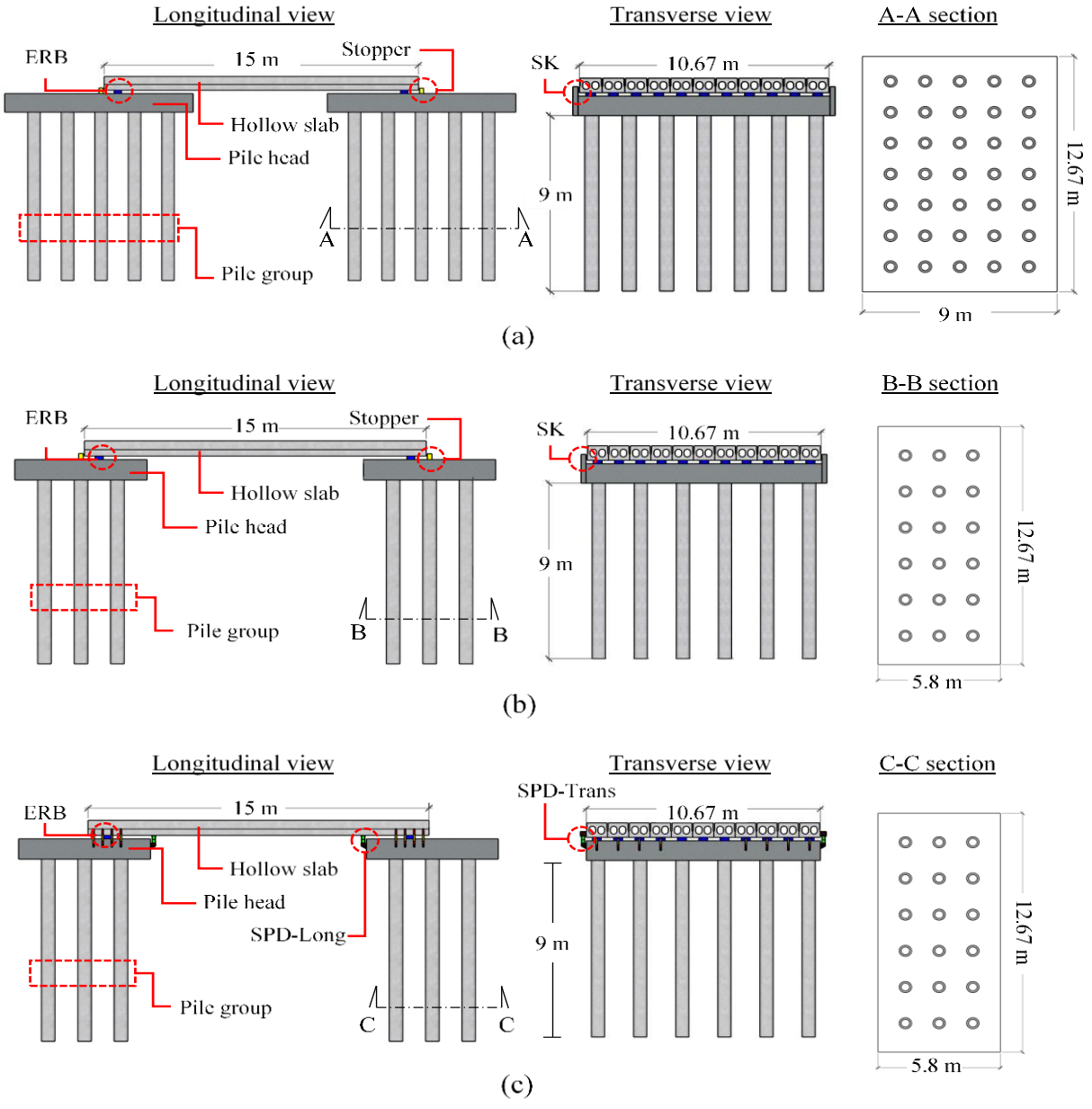

Figure 3. Overview of SHSPG Models: (a) SHSPG-A: (b) SHSPG-B: (c) SHSPG-C

Numerical Model of the Viaduct Structure

The structures were modeled as a single-span structure using STKO software. Mass and load of the inner span were implemented in each structure component as element mass and load. The mass and load of the outer spans were modeled as lumped mass and load. The spun pile was modeled as a displacement-based beam-column element. Gauss-Lobato integration method with five integration points was used in defining the plastic hinges of the pile. The pile element was modeled numerically using a fiber section. There were three structure models, namely SHSPG-A, SHSPG-B, and SHSPG-C. The SHSPG-A model was designed using an R-value of 1.5. The SHSPG-B model was designed using an R-value of 3.5. The SHSPG-C model was designed using an R-value of 3.5 with SPDs addition. The overview is shown in Figure 4.

The SHSPG-A structure used ERB devices according to DED, i.e., BS 250x400x41, while the SHSPG-B and SHSPG-C structures used smaller ERB devices, i.e., BS 200x250x52. The ERB devices were modeled elastically with multidirectional elastic stiffness and specific strain limit as summarized in Table 3. The elastic stiffness consists of vertical stiffness (E_v), horizontal stiffness (E_h), rotational stiffness ($E_{\theta\text{-}long}$ & $E_{\theta\text{-}trans}$), and torsional stiffness (E_t). The Δ_u was used to define the ultimate displacement of ERB which was calculated using its ultimate shear strain. Based on some literature, the ultimate shear strain of ERB could be determined with a value of 200% [13][14][15]. In order to prevent its ultimate shear strain, the stopper and shear key (SK) were usually used in conventional bridge structures. Then, both stopper and SK were used in the numerical models of SHSPG-A and SHSPG-B. On the other hand, the SHSPG-C was added with SPD devices that could minimize the ERB deformation so that it did not exceed its ultimate shear strain.

The application of SPD devices in SHSPG-C is shown in Figure 5. The material of SPD is a low-yield point steel LY225 with 191 MPa yield strength and 295 MPa ultimate strength [16]. The in-plane stiffness was modeled using bilinear model material, while the stiffnesses in other directions were modeled elastically as shown in Table 4. The simplified bilinear material model of SPD was adopted from equations for SPD bilinear model proposed by Chen, et. al. [17] as depicted in Figure 6 and summarized in Equation 1 to Equation 6. The equations had been verified by comparing the SPD behavior under cyclic loading in analytical and experimental tests by Chen, et. al. [18].

$$\gamma_y = \frac{\tau_y}{K} \quad (1)$$

$$\gamma_u = 20\gamma_y \quad (2)$$

$$\tau_y = \frac{\sigma_y}{\sqrt{3}} \quad (3)$$

$$\tau_u = \tau_w + \tau_f \quad (4)$$

$$\frac{\tau_w}{\tau_y} = 0.918 + \frac{0.038}{R_w^{\,2}} \leq 1.2 \quad (5)$$

$$\frac{\tau_f}{\tau_y} = 0.0287 \frac{b_f}{b_w} \cdot \frac{t_f}{t_w} \left(\frac{t_f}{t_w} \cdot \frac{1}{(n_L + 1) R_w \cdot \alpha} \right) \quad (6)$$

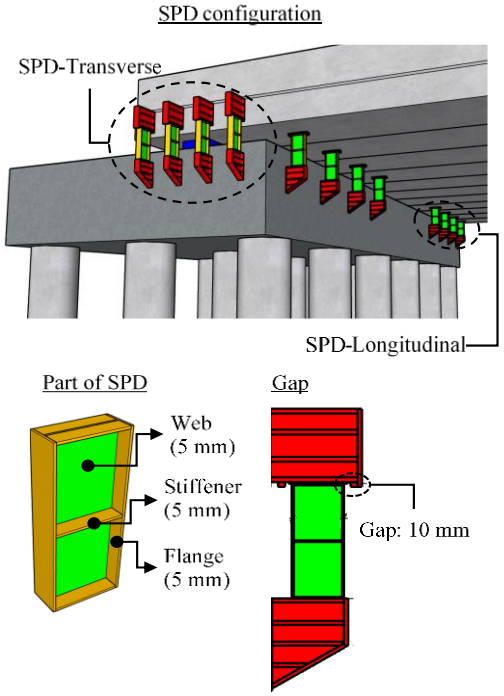

Figure 5. SPD Application in SHSPG-C Model

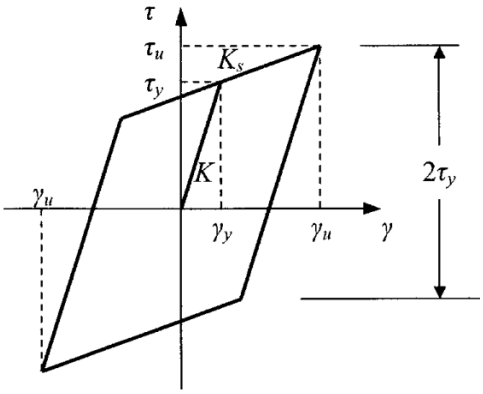

Figure 6. SPD Bilinear Model by Chen, et al. [17]

Table 3. Elastic Stiffness of ERB Devices in All Direction

Type of ERB	E_v (N/mm)	E_h (N/mm)	$E_{\theta\text{-}long}$ (Nmm)	$E_{\theta\text{-}trans}$ (Nmm)	E_t (Nmm)	Δ_u (mm)
BS 250x400x41	3.49×10^5	2.29×10^3	1.36×10^{10}	5.30×10^9	2.92×10^7	± 48
BS 200x250x52	8.97×10^4	8.59×10^2	1.04×10^9	6.63×10^8	5.88×10^6	± 64

Dynamic loads during the service life can cause fatigue failure of the SPD. It can be prevented by using a gap that can delay the work of the SPD so that the SPD will not experience any deformation during the service period [19,20]. The SPD will start working when the gap has been exceeded due to the earthquake excitation as shown in Figure 7. In this study, the designed gap distance was 10 mm, while the slab displacement due to dynamic service load was 7.56 mm. Thus, the gap was sufficient to delay the deformation of SPD devices.

Ground Motion Modeling

Ground motion modeling was carried out through four steps. First, the target spectrum was developed. It had been created while designing the structure. Second, seven pairs of earthquake data were selected [21]. The selection considered the similarity of the seismic mechanism and the proximity of the magnitude value to the specific location. Third, the recorded spectrums and ground motions were generated. Then, the recorded spectrums and ground motions were scaled and adjusted to the target spectrum of the structure location.

Table 4. SPD Material Properties

V_y (N)	K_s/K	K (N/mm)	Δ_{u+} (mm)	Δ_{u-} (mm)	E_v (N/mm)	E_h (N/mm)
80220	0.06	13555	54	-54	394000	100

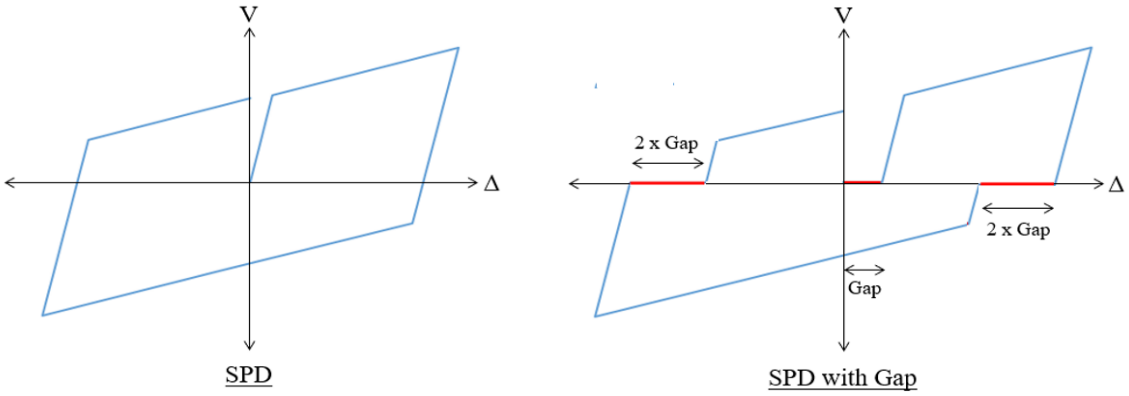

Figure 7. SPD with Gap Bilinear Model Idealization

Table 5. Selected Earthquake

No.	Earthquake	Year	Station	M_w	R [km]	Scale Factor Long	Scale Factor Trans
1	El Alamo	1956	El Centro Array #9	6.80	121.00	10.50	9.80
2	Big Bear	1992	Desert Hot Springs	6.46	39.52	2.70	3.50
3	Borrego Mtn	1968	El Centro Array #9	6.63	45.12	5.80	10.10
4	Imperial Valley	1979	Brawley Airport	6.53	8.54	5.50	2.50
5	Kobe	1995	Abeno	6.90	24.85	4.00	5.70
6	Kocaeli	1999	Ambarli	7.51	68.09	2.20	1.92
7	Superstition Hills	1987	Brawley Airport	6.54	17.03	6.00	8.00

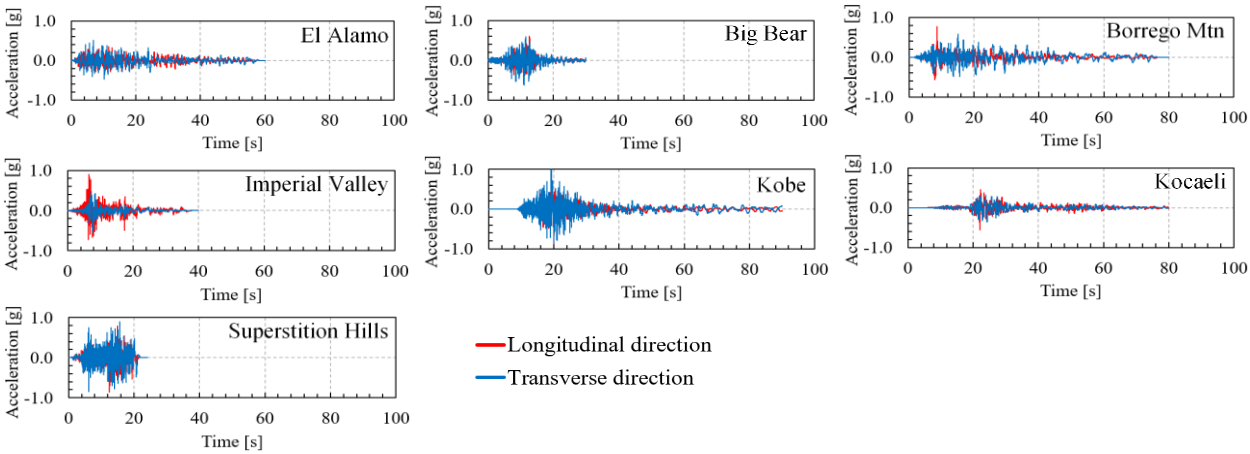

Figure 8. Scaled Ground Motion

The seismic mechanism of the Yogyakarta region was shallow crustal on the Opak fault with a strike-slip type and magnitude of 6.7-6.8 [22]. Due to the lack of data, the magnitude (M_w) of the selected earthquake could not be in the range of 6.7-6.8 precisely as shown in Table 5. Each selected earthquake data was scaled with a certain scale factor so that the average spectrum of the seven earthquakes was not below the target spectrum in the period range of $0.2T_1$ to $1.5T_1$. The T_1 is the natural period of the first mode of the structure. Based on modal analysis, the value of T_1 were 0.644 s for SHSPG-A, 0.989 s for SHSPG-B, and 0.978 s for SHSPG-C. Thus, the period of interest was 0.12-1.49 s. The scaled ground motions are depicted in Figure 8.

Limit State of Seismic Performance Level

The seismic performance level of the SHSPG structure consists of 3 levels, namely minimal damage (MD) level, controlled and repairable damage (CRD) level, and life safety protection (LSP) level [23]. Each level is limited by either the concrete strain or PC bar strain of the pile depending on which material reaches its strain limit first. Based on pushover analysis, the concrete material reached its limit strain before the PC bar for each performance level. The strain limits were converted to the displacement limits to make it easier to be observed as summarized in Table 6.

Table 6. Displacement Limit of the Seismic Performance Level

Level	Concrete Strain Limit	Pile Displacement Limit [mm]
MD	0.004	133
CRD	0.006	145
LSP	0.008	188

Result and Discussion

Pile Displacement Responses

The spun piles performed various displacement responses as shown in Figure 9. The displacement responses of SHSPG-B were greater than the other two. Moreover, some earthquakes caused residual displacement. The 35-piles stiffness of SHSPG-A which was greater than the 18-piles stiffness of SHSPG-B could minimize its lateral displacement responses. The application of eight SPDs in each direction in SHSPG-C could reduce the pile displacement response so that it was close to the pile displacement response of SHSPG-A.

The SHSPG-B structure experienced an increase in maximum displacement response of 158%-1002% in the longitudinal direction and 109%-822% in the transverse direction. Meanwhile, SHSPG-C showed a maximum displacement response of 61%-243% in the longitudinal direction and 70%-181% in the transverse direction. This indicated that the addition of the SPD devices to the "essential" structure could maintain its displacement response so that its value was still close to the displacement response of the "critical" structure.

Plastic Hinge Moment-Curvature

The most critical plastic hinge occurred at the top and bottom of the pile. The plastic hinge moment-curvature of the SHSPG-B pile was bigger than the moment-curvature of SHSPG-A and SHSPG-C piles as depicted in Figure 10. In SHSPG-A, the seismic force was distributed to 35 piles so that the bending moment of each pile was smaller than in SHSPG-B which was supported by 18 piles only. On the other hand, the bending moment of the SHSPG-C pile was smaller compared to the SHSPG-B pile because the earthquake energy had been dissipated by the SPD devices. Thus, the application of SPD devices could minimize the risk of plastic hinges.

Seismic Performances Level

Seismic performance levels of the SHSPG structure were classified according to the maximum displacement response of the piles. If the maximum displacement response of the pile was plotted onto the skeleton curve of the pile, the difference in the seismic performance level could be easier to be identified as shown in Figure 11. The skeleton curve was obtained from pushover analysis of a pile using the fixity depth idealization.

The seismic performance level of SHSPG-A was at the MD level. Based on the details of the post-earthquake visual condition of the structure in ASCE 61-14, the pile structure with MD level still behaves within elastic response. It experienced initial cracking and spalling of the concrete cover. However, it did not reduce the serviceability of the structure and no structural repair was needed.

The seismic performance level of SHSPG-B varied from the MD level to exceeding the LSP level limit. At the LSP level, the structure suffered more severe damage. The connection might be broken due to spalling into the concrete core. Unfortunately, 4 earthquakes in each direction caused the performance level to exceed the LSP limit. This could lead to a total collapse of the structure. Therefore, SHSPG-B posed a public hazard and should not be used in the design at this site.

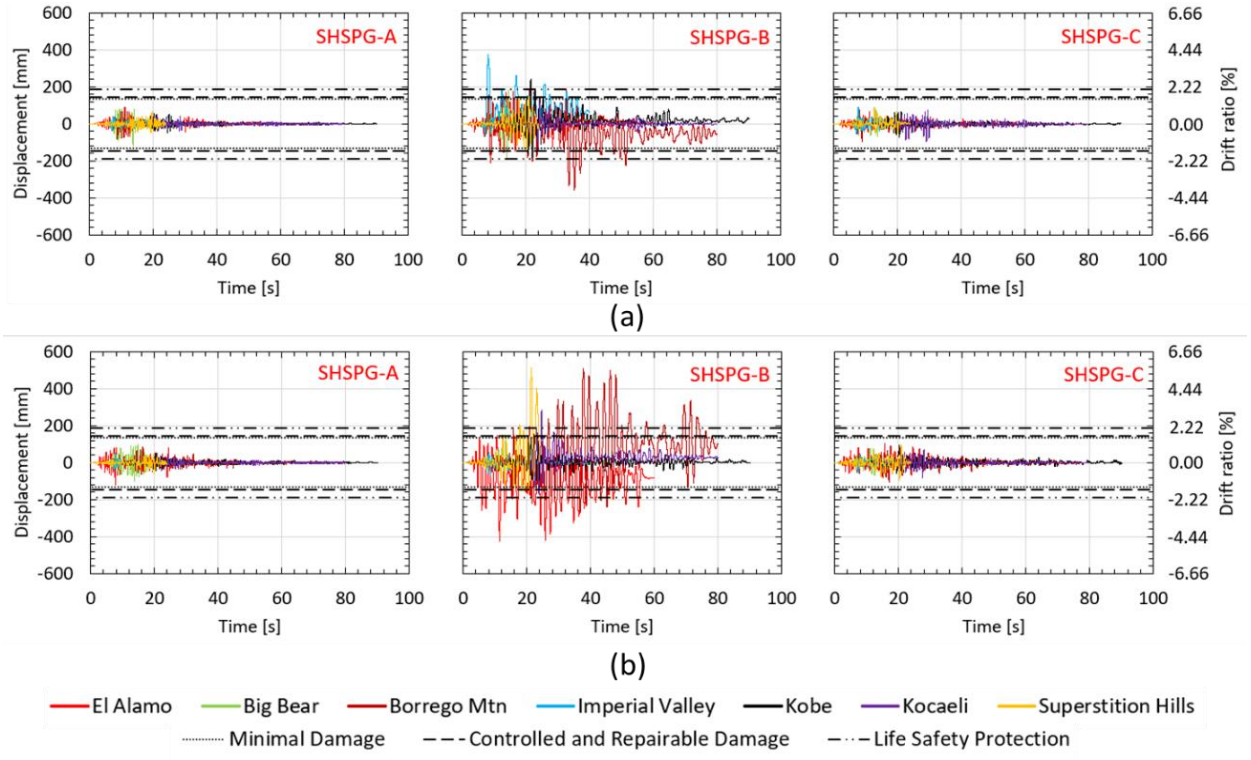

Figure 9. Displacement Responses: (a) Longitudinal Direction; (b) Transverse Direction

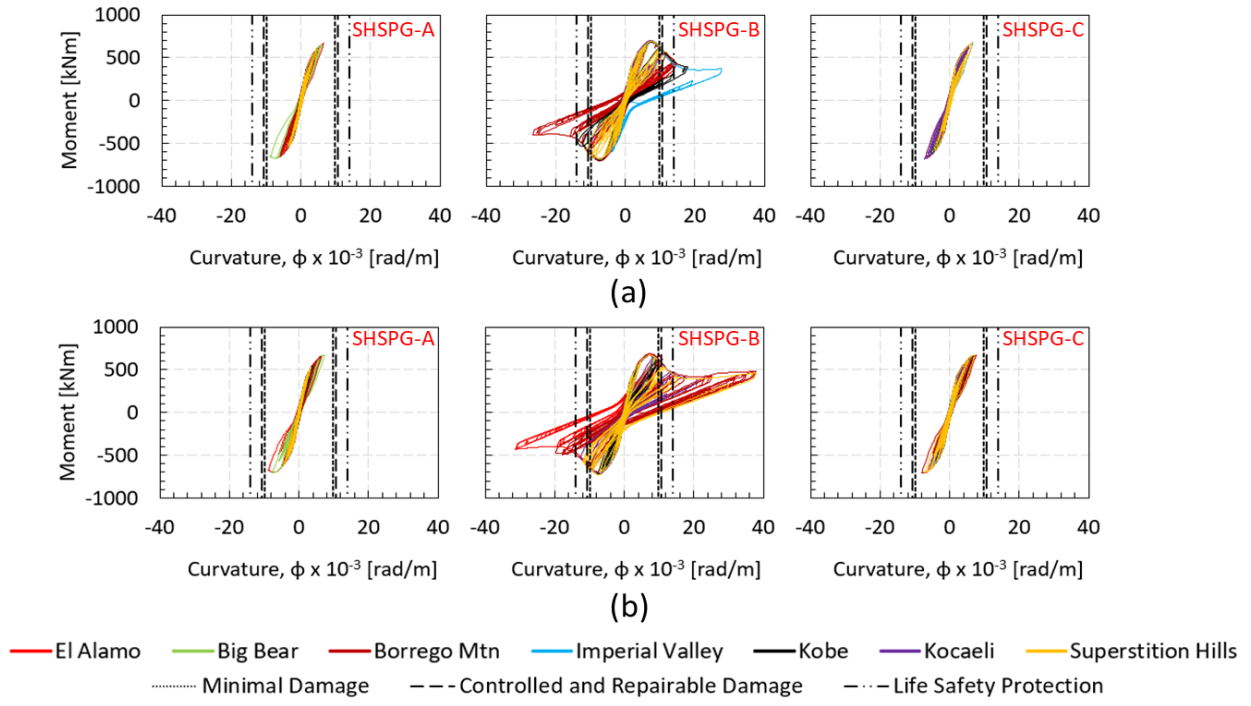

Figure 10. Moment-Curvature: (a) Longitudinal Direction; (b) Transverse Direction

The seismic performance level of SHSPG-C was MD level. This proved that the application of the SPD devices could maintain the seismic performance level of SHSPG-C so that it was the same as the SHSPG-A level. In conclusion, SHSPG-C could be an alternative SHSPG structure design at that location.

Elastomeric Rubber Bearing Responses

Based on NLTH analysis, the ERB devices had been exceeding the service limit of 50% shear strain. Maximum shear strains of ERB devices were 174.43% for SHSPG-A, 176.85% for SHSPG-B, and

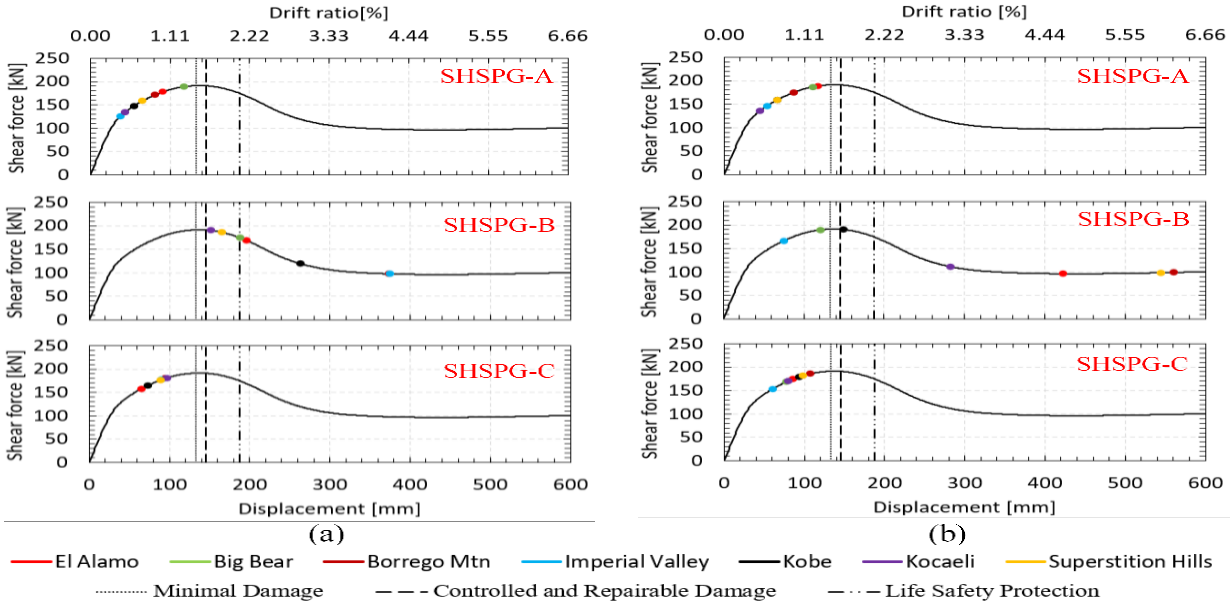

Figure 11. Seismic Performance Level: (a) Longitudinal Direction; (b) Transverse Direction

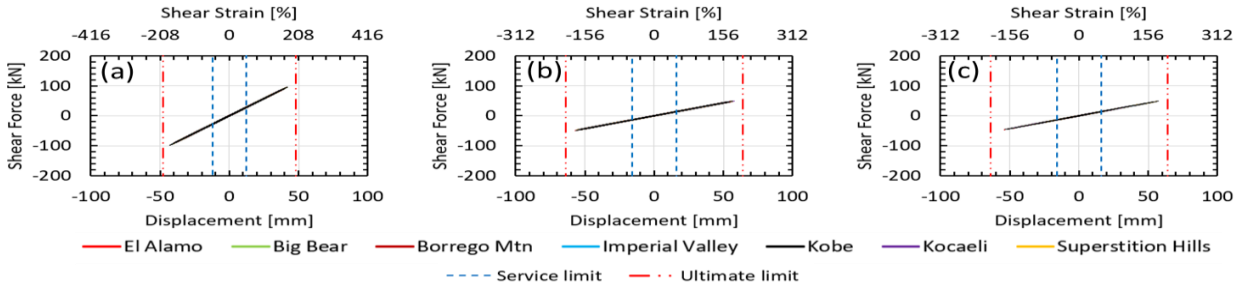

Figure 12. ERB Responses: (a) SHSPG-A; (b) SHSPG-B; SHSPG-C

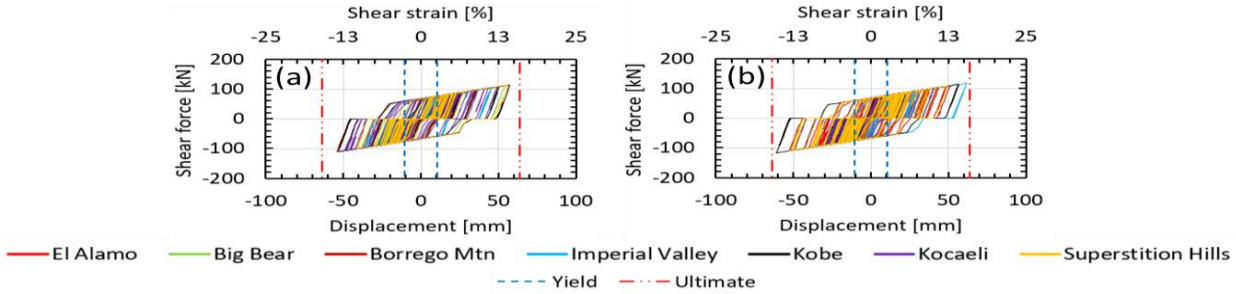

Figure 13. SPD Responses: (a) Longitudinal Direction; (b) Transverse Direction

192.74% for SHSPG-C as depicted in Figure 12. Even so, the shear strains were still under the ultimate limit so that the ERB devices did not experience sliding failure during the earthquake.

Shear Panel Damper Responses

According to the NLTH analysis result, the SPD shear strain was in the range of 6.94%-14.72% as shown in Figure 13. The shear strains were still in the range of the ultimate shear strain. In this range, the SPDs did not fall in rupture failure, but the shear strains were not much below the ultimate limit. Therefore, the SPD devices could perform optimally during an earthquake.

Hollow Slab and Pile Head Concrete Strain

The concrete strain of hollow slab and pile head structure should be checked to validate the elastic concrete material model assumption for both structures. Based on NLTH analyses, the concrete of the hollow slab experienced 0.000078 compression strain and 0.000079 tension strain, while the concrete of the pile head experienced 0.000005 compression strain and 0.000005 tension strain. The limit strains were 0.002 in compression and 0.000083 in tension. The concrete strain for hollow slab and pile head structures were still below the limit strain either in compression or in tension. Therefore, the concrete still behaved

elastically and the elastic concrete material model assumption for both structures were verified.

Structure Energy

Earthquake energy in the structure was distributed and converted into kinetic energy, viscous damping energy, plastic hinge energy, and hysteresis energy of seismic dampers [24] as shown in Table 7. The kinetic energy (KE) was calculated using the pile acceleration response. The viscous damping energy (VDE) was calculated using the pile velocity responses. The plastic hinge energy (PHE) was calculated using the plastic hinge moment-curvature. The hysteresis energy of the damper was calculated using SPD hysteresis energy (SHE).

The amount of kinetic energy was close to zero for all SHSPG structures. This was in accordance with another study by Kalkan & Kunnath [25]. In SHSPG-A, the proportion of viscous damping energy was 36.12%-49.95%, while the proportion of plastic hinge energy was 50.05%-63.88%. Although the plastic hinge energy proportion was greater than viscous damping energy, the values of both energies were still small. In SHSPG-B, the proportion of viscous damping energy was 39.75%-63.63%, while the proportion of plastic hinge energy was 36.37%-60.25%.

In SHSPG-C, both viscous damping and plastic hinge energy were reduced significantly. The viscous damping energy became 18.45%-22.21% and the plastic hinge energy became 27.96%-44.66%. It occurred due to the SPD hysteretic energy that performs in SHSPG-C with a contribution of 34.28%-53.09%. The SPD hysteretic energy was greater than the other energy for all earthquakes except Borrego Mtn-Long and Imperial Valley-Long. In both earthquakes, plastic hinge energy was greater than SPD hysteretic energy. However, the value of the plastic hinge energy of SHSPG-C for both earthquakes was much smaller than the plastic hinge energy of SHSPG-B. This means that the SPD application reduced the plastic hinge energy for both earthquakes, though the plastic hinge proportion was still greater than SPD hysteretic energy. Therefore, the SPD devices have a great

Table 7. Energy Distribution

Model	Earthquake	Direction	Energy [kJ]				Energy Percentage [%]			
			KE	VDE	PHE	SHE	KE	VDE	PHE	SHE
SHSPG-A	1	Long	0	607	982	-	0.00	38.21	61.79	-
		Trans	0	965	1524	-	0.00	38.78	61.22	-
	2	Long	0	836	1092	-	0.00	43.35	56.65	-
		Trans	0	1030	1397	-	0.00	42.45	57.55	-
	3	Long	0	576	886	-	0.00	39.38	60.62	-
		Trans	0	528	929	-	0.00	36.24	63.76	-
	4	Long	0	215	216	-	0.00	49.95	50.05	-
		Trans	0	93	164	-	0.00	36.12	63.88	-
	5	Long	0	481	500	-	0.00	49.00	51.00	-
		Trans	0	407	492	-	0.00	45.30	54.70	-
	6	Long	0	219	295	-	0.00	42.62	57.38	-
		Trans	0	150	248	-	0.00	37.65	62.35	-
	7	Long	0	422	516	-	0.00	45.05	54.95	-
		Trans	0	324	378	-	0.00	46.35	53.65	-
SHSPG-B	1	Long	0	1493	1333	-	0.00	52.83	47.17	-
		Trans	0	2923	1782	-	0.00	62.13	37.87	-
	2	Long	0	686	909	-	0.00	42.99	57.01	-
		Trans	0	308	429	-	0.00	41.81	58.19	-
	3	Long	0	2086	1659	-	0.00	55.73	44.27	-
		Trans	0	4885	2792	-	0.00	63.63	36.37	-
	4	Long	0	629	762	-	0.00	45.28	54.72	-
		Trans	0	155	172	-	0.00	47.33	52.67	-
	5	Long	0	1111	1117	-	0.00	49.95	50.05	-
		Trans	0	745	1053	-	0.00	41.44	58.56	-
	6	Long	0	464	704	-	0.00	39.75	60.25	-
		Trans	0	841	1030	-	0.00	44.94	55.06	-
	7	Long	0	729	890	-	0.00	45.02	54.98	-
		Trans	0	1601	1668	-	0.00	48.97	51.03	-
SHSPG-C	1	Long	0	306	448	622	0.00	22.21	32.56	45.23
		Trans	0	447	697	1079	0.00	20.12	31.34	48.54
	2	Long	0	185	285	495	0.00	19.20	29.50	51.30
		Trans	0	250	369	700	0.00	18.95	27.96	53.09
	3	Long	0	198	419	322	0.00	21.06	44.66	34.28
		Trans	0	474	811	927	0.00	21.43	36.67	41.90
	4	Long	0	150	263	262	0.00	22.27	38.98	38.75
		Trans	0	76	115	159	0.00	21.78	32.80	45.42
	5	Long	0	227	356	647	0.00	18.45	28.95	52.60
		Trans	0	297	505	595	0.00	21.27	36.14	42.59
	6	Long	0	379	608	887	0.00	20.23	32.45	47.32
		Trans	0	238	391	544	0.00	20.32	33.34	46.34
	7	Long	0	173	265	403	0.00	20.55	31.53	47.92
		Trans	0	288	450	716	0.00	19.82	30.95	49.23

contribution in dissipating energy and minimizing the damage of the main structure.

Conclusion

The application of SPDs to the "essential" SHSPG viaduct with an R-value of 3.5 could maintain its seismic performance at the MD level which was the same level as the "critical" SHSPG viaduct with an R-value of 1.5. In addition, the displacement response and the plastic hinge moment-curvature also could be kept within elastic zone. The application of SPD devices achieved 34.28%-53.09% energy dissipation of the structure during the earthquake.

Acknowledgment

The authors would like to express their gratefulness for the data and financial support provided by the Department of Civil and Environmental Engineering Universitas Gadjah Mada; Directorate General of Higher Education, Research, and Technology MOECRT Indonesia; PT. Wika Beton, Tbk.; and PT. Raya Konsult.

References

1. Yeung, A.T., Installation of Prestressed Spun High Strength Concrete Piles by Hydraulic Jacking, in *The HKIE Geotechnical Division Annual Seminar*, 2014, pp. 109–115.
2. Budek, A. M., Benzoni, G., and Priestley, M.J.N., *Experimental Investigation of Ductility of In-Ground Hinges in Solid and Hollow Prestressed Piles*, Structural Systems Research Project, University of California, San Diego, 1997.
3. Irawan, C., Djamaluddin, R., Raka, Faimun, I.G.P., Suprobo, P., and Gambiro, Confinement Behavior of Spun Pile Using Low Amount of Spiral Reinforcement - An Experimental Study, *International Journal Advenced Science Engineering Infrastucture Technoly*, 8(2), 2018, pp. 501–507, doi: 10.18517/ijaseit.8.2.4343.
4. Setiyono, U. *et al.*, *Katalog Gempa Bumi Signifikan dan Merusak 1821-2018*, 1st ed. Jakarta Pusat: Pusat Gempa Bumi dan Tsunami BMKG, 2019.
5. Darmawan, M.F., *Pile-Supported Slab Viaduct Structure Braced With Shear Panel Damper*, Universitas Gadjah Mada, 2021.
6. Xu, L.Y., Nie, X., and Fan, J.S., Cyclic Behaviour of Low-yield-point Steel Shear Panel Dampers, *Engineering Structure*, 126, 2016, pp. 391–404, doi: 10.1016/j.engstruct.2016.08.002.
7. Yang, L., Gao, Y., Shi, G., Wang, X., and Bai, Y., Low Cycle Fatigue Property and Fracture Behavior of Low Yield Point Steels, *Construction Building Material*, 165, 2018, pp. 688–696, doi: 10.1016/j.conbuildmat.2018.01.075.
8. Abebe, D.Y., Kim, J.W., Gwak, G.,and Choi, J.H., Low-Cycled Hysteresis Characteristics of Circular Hollow Steel Damper Subjected to Inelastic Behavior, *International Journal Steel Structure*, 19(1), February 2019, pp. 157–167, doi: 10.1007/s13296-018-0097-8.
9. Menteri Perhubungan Republik Indonesia., *Persyaratan Teknis Jalur Kereta Api*. Jakarta: Menteri Perhubungan Republik Indonesia, 2012.
10. BSNI., *Perencanaan Jembatan Terhadap Beban Gempa SNI 2833*, Jakarta: BSNI, 2016.
11. AASHTO., *AASHTO LRFD Bridge Design Specification*. 2012.
12. Kent D.C. and Park, R., Flexural Members with Confined Concrete, *Journal Structure Division*, 97(7), 1971, doi: 10.1061/JSDEAG.0002957.
13. The European Union., *Eurocode,* 8(8). 2011.
14. Furuta, T. and Araki, S., The Horizontal Deformation Characteristics of Natural Rubber Bearing by FEM Analysis, in *13th World Conference on Earthquake Engineering*, 2004, 78, pp. 41–49, doi: 10.5459/bnzsee.38.1.41-49.
15. Han, X., Kelleher, C.A., Warn, G.P., and Wagener, T., Identification of the Controlling Mechanism for Predicting Critical Loads in Elastomeric Bearings, *Journal Structure Engineering*, 139(12), 2013, pp. 1–12, doi: 10.1061/(asce)st.1943-541x.0000811.
16. Shi, G., Gao, Y., Wang, X., and Zhang, Y., Mechanical Properties and Constitutive Models of Low Yield Point Steels, *Construction Building Materials*, 175, 2018, pp. 570–587, doi: 10.1016/j.conbuildmat.2018.04.219.
17. Chen, Z., Ge, H.,and Usami, T., Hysteretic Model of Stiffened Shear Panel Dampers, *Journal Structure Engineering*, 132(3), 2006, pp. 478–483, doi: 10.1061/(asce)0733-9445(2006)132:3(478).
18. Chen, Z.Y., Chen, W., and Bian, G.Q., Seismic Performance Upgrading for Underground Structures by Introducing Shear Panel Dampers, *Advanced Strucural Engineering*, 17(9), 2014, pp. 1343–1357, doi: 10.1260/1369-4332.17.9.1343.
19. Setiawan, A.F., *Development of High Seismic Performance Ingegrated Bridge Pier Connected by Hysterical Damper,* Kyoto, 2018.
20. Setiawan, A.F., Takahashi, Y., and Sawada, S., Development of a Shear Panel Damper Plus Gap, *Journal JSCE*, Under Review, 2018, pp. 1–13.
21. ASCE., *Minimum Design Loads and Associated Criteria for Buildings and Other Structures. Structural Engineering Institute of the American Society of Civil Engineering, Reston*, no. 7 98. Virginia: American Society of Civil Engineers, 2013.
22. Sunardi, B., Percepatan Tanah Sintetis Kota Yogyakarta Berdasarkan Deagregasi Bahaya Gempa, *Jurnal Lingkungan dan Bencana Geology*, 6(3), 2015, pp. 211–228.
23. ASCE and COPRI., *Seismic Design of Piers and Wharves*. Virginia: ASCE, 2014.
24. Uang, C. and Bertero, V.V., Evaluation of Seismic Energy in Structures, *Earthquake Engineering & Structural Dynamics*, 19(1), 1990, pp. 77–90, doi: 10.1002/eqe.4290190 108.
25. Kalkan, E. and Kunnath, S.K., Effective Cyclic Energy as a Measure of Seismic Demand, *Journal of Earthquake Engineering,* 11(5), 2007, pp. 725–751, doi: 10.1080/13632460601033827.